Transparent ceramics green-microstructure optimization by pressure slip-casting: Cases of YAG and MgAl2O4

Rémy Boulesteix, Adrian Goldstein, Camille Perrière, Alexandre Maître, Mickael Katz, Christophe Coureau, Christian Sallé

Transparent ceramics green-microstructure optimization by pressure slip-casting: cases of YAG and $MgAl_2O_4$

Rémy Boulesteix[1*], Adrian Goldstein[2], Camille Perrière[1], Alexandre Maître[1], Mickael Katz[2], Christophe Coureau[3], Christian Sallé[4]

[1] Institute for Research on Ceramics (IRCER), UMR CNRS 7315, Univ. Limoges, F-87068 Limoges, FRANCE

[2] Israel Ceramic and silicate institute (ICSI), Technion City, 32000 Haifa, ISRAEL

[3] SOLCERA, F-45063 Evreux, FRANCE

[4] CILAS, F-45100 Orléans, FRANCE

Abstract:

This paper presents experimental data and its interpretation regarding the forming of YAG and spinel green-bodies, intended for transparent parts fabrication, by the pressure slip casting (PSC) method. Conditions for an optimal operation are established based on the modeling of the filtration kinetics. It emerges that the method is able to provide highly sinterable green parts by ensuring that the cakes porosity exhibits low average size and narrow size distribution. Results were compared with other popular forming approaches like slip casting (SC) and cold isostatic pressing (CIP). PSC was found as superior, to the other approaches, as far as obtainment of high sinterability green- bodies is concerned. In the case of YAG, it was shown that PSC method even allows the replacement of the traditional long vacuum firings by a two stage densification operation in which an initial air-firing is completed by a hot isostatic pressing step.

Keywords: Transparent ceramics, YAG, spinel, pressure slip casting, HIP

1. Introduction

Transparent ceramics (TC) manufacturing optimization is understudy worldwide owing to their interesting applications [1,2]. The main technological difficulty, in this domain, is the ensuring of the really high level of densification required, for transparency achievement; higher than that needed by any other advanced ceramics. For example, in the case of products like transparent armor the admissible remnant porosity is as low as ~ 100 vol. ppm while for gain-media, used in high power solid-state lasers, this drops further to under 5 vol. ppm [3].

It was gradually realized that the key, for achieving the necessary near-full densification, is a suitable microstructure of the specimens in their green-state [1–7]. As a result of this realization, the early focus on sintering of the engineering studies devoted to transparent ceramics is now replaced by a broader scope approach, in which more attention is attributed to processing before firing. The main features of a high-sinterability powder compact are a low and narrow distribution size of the pores and such a configuration has to be strictly maintained over all the macroscopic volume of the specimens: microcracks, virtual delamination surfaces and residual mechanical stress need to be quasi-absent [1]. In order to achieve in practice the desired green-body configuration, the powder preparation, processing and forming stages need to be optimized and correlated so as to ensure a proper management of the powder aggregates comminution and a uniform compact arrangement of the particles resulting from aggregates breaking.

In this context, as demonstrated long ago by F.F. Lange or A. Roosen and H.K. Bowen among others, forming methods which use liquid suspensions exhibit certain advantages over methods working with dry systems, especially regarding the aggregates breaking and material flow processes active during forming operations [8,9]. The main reason for that is the fact that in liquid suspension a highly dispersed state can be maintained during all the duration of the forming operation, more easily than in dry systems. Slip-casting (SC) is the most ubiquitous

liquid state based forming method [10,11]. However, in its conventional variant, *i.e.* casting in plaster of Paris molds at atmospheric pressure, it generally produces green-bodies having limited thickness because of long filtration time and plaster saturation by water. Also the use of plaster molds can induce contamination of the green bodies (especially by Ca^{2+} ions and/or $CaSO_4$ particles) and molds working life is limited. Owing to the variable and large average size of pores in the plaster of Paris and the weak suction force (does not force compact arrangement of cake particles), the conventional SC casting kinetics are slow and thus needs very stable dispersed state of the suspension until the end of the casting. However, experiments showed that if optimal casting conditions are ensured the method is able to generate highly sinterable green-bodies, as posited by Lange et al. For instance, slip casting stands up to expectations when used in its pressure-assisted (PSC) format. The PSC is an established method but used mostly in metallurgy or ceramic tableware and refractories manufacture [12–19]. Lately, it was shown as being attractive also for the case of some transparent ceramics fabrication [20–23]. For a more complete demonstration of PSC`s abilities, in this domain, comparison with other forming techniques is necessary. Such comparison is rarely, if at all, provided by the literature on transparent ceramics processing, but one can notice the research work of Krell *et al.* in this domain [5,24]. A full understanding of the reasons which make PSC advantageous, especially in the case of transparent ceramics manufacturing, is still lacking.

Owing to the above, in the work described by this paper, a PSC procedure – optimized based on the results of a modelling assisted study of the process` kinetics – was used to form green bodies of YAG and spinel. For comparison, specimens were also consolidated by isostatic cold isostatic pressing (CIP) and by conventional atmospheric slip casting (SC). The objective was to compare the three methods, especially regarding their ability to generate sinterable green-bodies. For attaining the objective, their microstructural characteristics – which

determine their sinterability – were measured. Further the relative density and spectral characteristics of densified specimens were also measured and compared. The results were discussed from the point of view of sinterability.

2. Experimental

2.1. Spinel ceramics

2.1.1. Raw materials

In the case of spinel, the raw-material ~~(powder denominated *SPI-P1*)~~ is the grade S30-CR of Baikowski (La Balme de Sillingy, France), prepared from a pure aluminum and Mg sulphate, by a colloidal chemistry method; the calcine is thoroughly jet-milled and contains spinel ($MgAl_2O_4$, cubic) as the only phase detectable by XRD examination. It also has a reasonable elemental purity (around 200 ppm of Ca, Fe, Na, K) except its S content which varies in the 200 to 600 ppm (sulfur as major impurity may confer a parasitic yellow tint to sintered parts [23]). The powder has a specific surface area (SSA) of 28-30 $m^2 \cdot g^{-1}$. The basic particles (40-80 nm in diameter) have an isotropic shape and are agglomerated as illustrated in Figure 1a,c. The phase composition of the powder is shown in Figure 1b while the particle size distribution of the as-received powder is presented in panel d of Figure 1. ~~This powder was used in the SC and PSC experiments. A second powder (*SPI-P2*) was derived, by processing the main SPI-P1 material, for CIPing experiments (see 2.2).~~

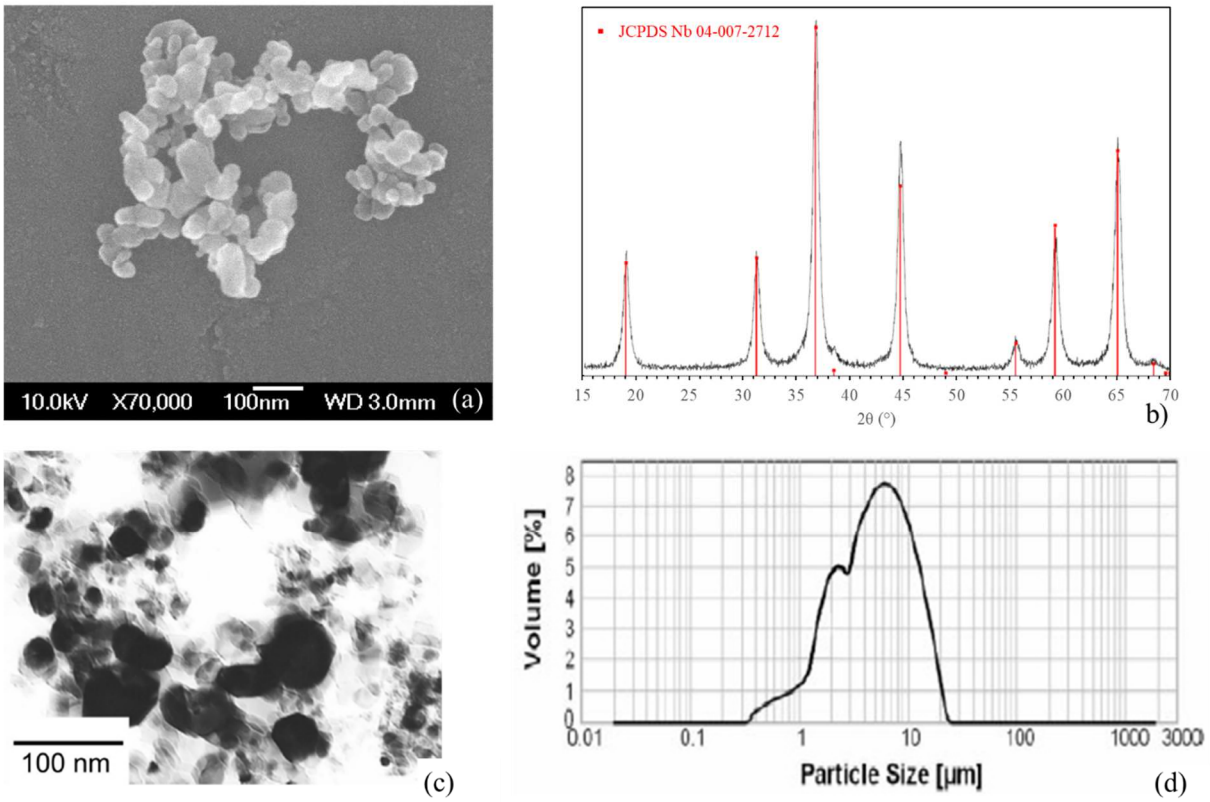

Figure 1: (a) FEG-SEM micrograph, (b) XRD pattern, (c) TEM micrograph and (d) particle size distribution of as-received spinel powder SPI-P1.

The as-received powder was further milled in a desk-top attritor type mill (Netzsch-Feinmahltechnick, Selb, Germany) working at 1300 rotations per minute (lined with polymer and including a polymer disc) by the aid of super-dense, low wear alumina 2 mm balls (IKTS, Dresden, Germany). The suspending medium was iso-propyl alcohol and operation time 25 min. The particle size distribution after attrition milling is presented in Figure 2. Ready-to-press material **(*i.e.* only used for CIP)** was derived from the milled and dried powder by subjecting it to granulation by forcing passing through 72 mesh sieve for producing rounded shape soft granules.

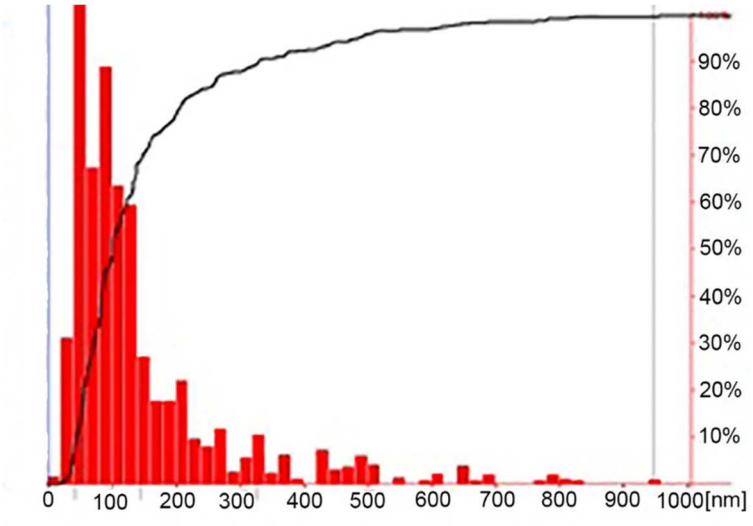

Figure 2: Particle size distribution in volume of spinel powder ~~***SPI-P1***~~ *after milling.*

2.1.2. Green-bodies forming

Most of the specimens were disc shaped having, in their green-state, diameters between 25 and 60 mm and thickness in the 3 to 6 mm range. They were formed by cold isostatic pressing (CIP), SC and PSC.

For CIPing, **the milled, dried and granulated Spinel powder was used.** A pressing schedule in two stages was used. After shaping in steel dies at low uniaxial pressure (10 MPa) the discs placed in vacuumed bags were subjected to a CIPing stage in which pressure was gradually increased to 120 MPa and kept constant for a five minutes dwell; pressure release was also effectuated with short stops at 80 and 50 MPa; the procedure significantly reduces formation of macro defects like voids.

For simple slip-casting a water suspension of the **raw Spinel** powder was introduced into a planetary mill, made of alumina, together with a few polymer made balls (20-30 min of operation). With the aid of $C_6H_8O_7$ (**0.4wt.%** of 2-hydroxypropane-1,2,3-tricarboxylic acid) as a defloculant, stable suspensions of 79wt.% solid load could be prepared. The suspensions

were cast into a die having a metal wall and a plaster of Paris base; drying was effectuated keeping the casts at room temperature for four days.

~~**The forming by the PSC approach was similar to that used for YAG and will be described below.**~~ **In the case of PSC forming, the raw powder was dispersed in deionized water with 30vol.% of solid load and 1.2wt.% of PAA (Ammonium polyacrylate) as dispersant. Suspensions were ball-milled with corundum balls of 2 mm in diameter in order to obtain homogeneous slurries. Discs were formed by pressure filtration with the same protocol described below for YAG ceramics.**

2.1.3. Sintering

The spinel densification was effectuated by a two-step method. A first step consisted in pressureless pre-sintering and was conducted under air (AS) in a muffle furnace (model RT-1800 furnace, C&M, Bloomfield, NJ, US). They were effectuated at various temperatures located in the 1480°C to 1680°C interval in order to identify the optimal conditions. The task of the first stage was to ensure a fired state relative bulk density (BDf) of 97-98% of the theoretical density (TD) and a close to zero open porosity (OP). The second stage consisted in post-densification by Hot Isostatic Pressing (post-HIP) and was effectuated in a model AIP6-30H machine, of AIP, Columbus, OH, US. It includes graphite components (thus carbon in its atmosphere) and operates under 200 MPa of Ar at 1800°C for 5 h.

2.2. YAG ceramics

2.2.1. Raw materials

In the case of YAG, two different powder sources were used **to illustrate on one hand, the influence of powder characteristics (particles size, agglomeration state, etc.) and, on the**

other hand, the influence of the shaping and sintering process. Therefore, the results and final conclusions were expected to be more universal and reliable. Their densification was accomplished by the aid of a reaction-preceded sintering procedure (*i.e.* during the thermal treatment, the reaction between primary oxides powders occurs before the densification of YAG phase). For the first tests (powder denominated ***YAG-P1***), the raw-materials were Al_2O_3 (grade HP-DBN of Reynolds Works, Malakoff, TX, US) and Y_2O_3 (grade 3N of AMR, Toronto, Canada). The alumina powder is a 4N purity material, having as its main impurity 45 ppm of Fe. It has a d_{50} = 0.5 µm and a SSA = 9 $m^2 \cdot g^{-1}$. The yttria powder has as main impurities Si, Ce, Fe and Cr (< 100 ppm) and a d_{50} = 0.6 µm. Sintering aid Si was introduced as TEOS (> 98% purity, Merck, Hohenbrum, Germany); the amount was equivalent with a 0.5 wt.% SiO_2 content.

For the second set of tests on YAG ceramics (powder denominated ***YAG-P2***), commercial submicrometric α-Al_2O_3 (Ø < 0.5 µm; purity > 99.99%, Baïkowski, Poisy, France), Y_2O_3 (Ø < 0.5 µm; purity > 99.99%, Solvay, La Rochelle, France), and Nd_2O_3 (Ø < 1 µm; purity > 99.99 %, Alfa Aesar, Kendel, Germany) were used. 1 at.% Nd was introduced to obtain 1 at.% Nd:YAG transparent ceramics after sintering.

2.2.2. Green bodies forming

For CIPing, the raw powders were first de-agglomerated and mixed by processing in an attritor mill (with parameters similar than for spinel powder) and then further mixed in a planetary mill (10 min with polymer balls in iso-propyl alcohol containing 0.8wt.% alcohol ethoxylate and 1wt.% PEG 400) with the TEOS solution. The product was dried at room-temperature and then granulated according to the protocol described above for spinel. The obtained powder was subjected to pressing according to the same protocol as spinel. After shaping in steel dies at low uniaxial pressure (50 MPa) the discs placed in

vacuumed bags were subjected to a CIPing stage in which pressure was gradually increased to 100 MPa and kept constant for a five minutes dwell.

In the case of **SC and** PSC forming (YAG-P1 and P2 derived), the initial oxides were blended together in deionized water with 30vol.% of solid load and 1.2wt.% of PAA (Ammonium polyacrylate) as dispersant. Suspensions were ball-milled with corundum balls of 2 mm in diameter in order to obtain homogeneous slurries with quasi-Newtonian behaviour and a viscosity of 20 mPa.s at a shear rate of 100 s^{-1} [20]. The viscosity was measured over time and was found to be quite constant at 20°C for at least 72 h. 1at.% Nd was introduced to obtain 1at.% Nd:YAG ceramics after the sintering process. **For Simple SC, the suspensions were cast into a die having a metal wall and a plaster of Paris base; drying was effectuated keeping the casts at room temperature for four days. For PSC, discs or barrels** were formed by pressure filtration at 2-3 MPa under nitrogen gas pressure with the home-made apparatus described in Figure 3. The casting process was optimized as described in the section 3.1.1. Details about the casting operation **and slurry characteristics** may be found in [20]. After drying at room temperature under air atmosphere for several days, samples were calcined under air at T < 900°C to remove organic residues.

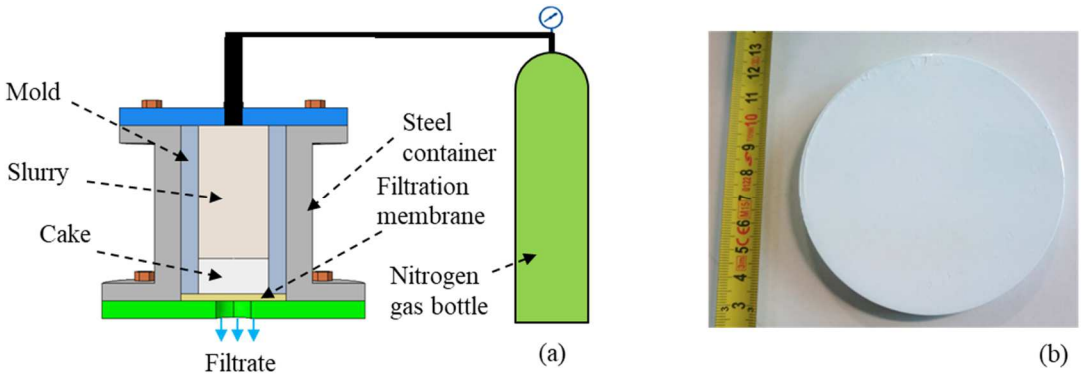

Figure 3: Scheme of the pressure slip-casting (PSC) apparatus (a). Example of green compact of YAG (from YAG-P2 powder), 100 mm in diameter and 10 mm thick, manufactured by PSC (b).

2.3. Sintering

YAG specimens were sintered according to two different ways. In the first procedure **(used for samples derived from YAG-P2 powder)**, sintering was performed by pressureless sintering under vacuum (VS) at a temperature of 1700°C for 20 h with heating and cooling rates of 5°C·min^{-1}. Sintering was conducted in a tungsten mesh-heated furnace under secondary vacuum ($P < 10^{-2}$ Pa). Specimens were placed in an alumina crucible.

The second procedure **(used for samples derived from YAG-P1 powder)** used two stages **(*i.e.* air presintering + post-HIP) as described above for spinel**.

2.4. Characterizations

The particle size distribution of the powders (PSD) was measured by the aid of both a model LA-950A2 (Horiba, Kyoto, Japan) machine for as-received powders and a model LM-20 (Nanosight Tech., Salisbury, UK) for the attritor milled powder because particle size drops down to under 1 micrometer range. The pore size distribution (P_oSD) was determined by mercury intrusion (model Poremaster 60, Quantachrome, Instruments, Boyton Beach, FL, US). Green compacts were also characterized by high resolution X-Ray microtomography (Versa 500, Zeiss, Oberkochen, Germany) with a 150 nm spatial resolution. Densification behaviour during thermal treatment under vacuum was examined by using a thermo-mechanical analyzer (TMA Setsys evolution, Setaram, France) with heating rate of 5°C.min^{-1} ($P \leq 10^{-2}$ Pa).

After sintering, the optical transmission spectra were recorded with a model Lambda 950 spectrophotometer fabricated by Perkin-Elmer (Shelton, CT, US). Prior to analysis, specimens were mirror polished into discs with a thickness of 2 mm. In order to record only the region of the beam relevant for the so called **real in-line transmission (RIT, *i.e.* transmittance without the scattered light)** a 4×4 mm slit was placed between the light source and detector.

The defects in the volume of samples were imaged by photos taken with an optical transmission microscope (Ortholux 1-pol, Ernest Leitz Gmbh, Wetzlar, Germany). Also, optical tomography was performed on transparent samples by confocal laser scanning microscopy (CLSM, LSM 510META, Zeiss, Germany) according to a method described elsewhere [25]. Chemical analyses of the samples surface after sintering were also performed by electron microprobe analysis (EMPA) (Quanta 200, FEI, Eindhoven, NL) to which an X-ray fluorescence analyzer of Oxford Instruments (Tubney Woods, UK) was attached. Structural analyses were performed by X-ray diffraction (XRD) (APD 1000, ItalStructures, Riva del Garda, Italy). The sintered state bulk density was measured by the conventional, Archimedes principle based, technique in water.

3. Results

Below, first, the results received are presented in distinct sections for YAG and spinel. **It is worth to notice here that the results were discussed in terms of samples microstructural features rather than powders characteristics. In fact, it would not be easy to separate the exact role of powder characteristics to the shaping process parameters because they strongly depend to each other. Finally, the last section of the Chapter is devoted to an integrated discussion of the results obtained for both materials.**

3.1. YAG-based ceramics

3.1.1 Study of PSC kinetics

At first, YAG-P2 green compacts were shaped by PSC under various gas pressures. Samples thickness was recorded as a function of time and obtained data were reported in Figure 4a. The higher is the applied pressure the faster is the cake thickness formation. This effect of the magnitude of the applied pressure on the PSC kinetics was already described in many previous works [14,18,19].

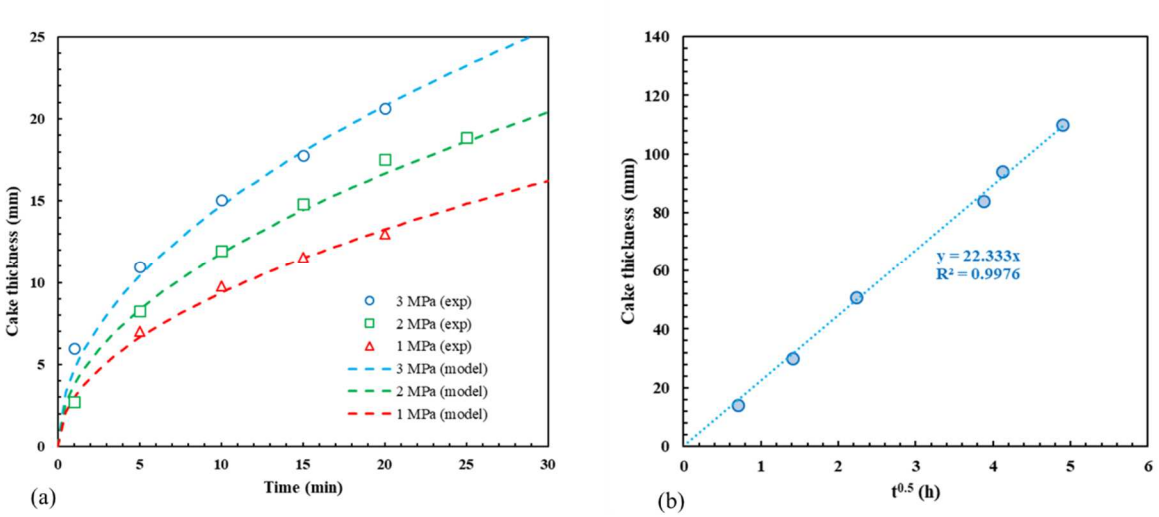

Figure 4: Pressure slip casting kinetics (cake thickness as a function of time) as a function of the applied gas pressure (a). Pressure slip casting kinetics for a longer time (24 h) under a pressure of 3 MPa in reduced coordinate $t^{0.5}$ (b). Experimental data (symbols) were fitted by Darcy's model (dotted lines).

As shown in Figure 4, a good agreement between experiments and analytical model was found when data were fitted by simple Darcy's model. In fact, by applying the mass balance to the PSC system, and integrating the Darcy's equation, the following equation (Eq. (1)) is obtained relating the thickness of the cake (x) with casting time (t):

$$x^2 = \frac{2k\Delta p}{\eta}\left(\frac{\rho_s}{\rho_c - \rho_s}\right)t \qquad \text{Eq. (1)}$$

where k is the permeability of the cake, Δp the applied pressure, η the viscosity of the solvent of suspensions (water in this case), ρ_s the suspension density and ρ_c the cake density. That means, the filtrate flow through the cake, constituted by the stacking of particles on a porous surface, can be described by similar equations generally encountered in classical filtration [26,27]. Such result is very useful to predict the cake thickness at a given time. Moreover, the casting kinetics can be related to cake microstructural features like pore size distribution and can be useful for the control and optimization of ceramics microstructure [14,20].

Applying the results described above to the casting process optimization, it was possible to define casting conditions allowing the forming of samples of 20 mm in thickness in pretty short time (*i.e.* 20 min under 3 MPa, see Figure 4a). That is generally not so easy with colloidal suspensions containing submicrometric particles (*i.e.* "nanopowders"). In fact, according to Ergun's law, the fluid flow across a porous network decreases with pore size, quite rapidly as Eq. (2) indicates [28–30]:

$$k = \frac{\varepsilon^3 {d_p}^2}{150(1-\varepsilon)^2} \qquad \text{Eq. (2)}$$

where d_p is the mean diameter of pores in the cake (in m) and ε the total porosity fraction ($0 < \varepsilon < 1$).

Thus, owing to these first encouraging results, it was decided to test the feasibility of thicker YAG pieces (*i.e.* x > 50 mm) by PSC. The thickness of the parts obtained was measured for different filtration times until 24 h. Quite surprisingly, measured data were also well fitted by Darcy's law for the whole process time (*i.e.* 24 h, very long compared to usual), as depicted in Figure 4b. As a result, it was possible to obtain green parts with a thickness as high as 110 mm for 24 h of filtration time. That means the cake microstructural features (pore size distribution and density) should be very stable over time as it will be verified in the section 3.1.2. One have to mention that such results were obtained only after an optimization of slurry formulation ensuring enough stability, *i.e.* constant viscosity and no sedimentation for at least 72 h (see section 2.2).

This filtration model based on Darcy's law was implemented in COMSOL® software in order to describe and predict the velocity field of the suspension and the filtrate, as well as the static pressure in the entire simulated zone (*i.e.* suspension and cake in the mold). **~~The results obtained for 1 at.% Nd:YAG suspension are illustrated in~~** ~~Erreur ! Source du renvoi introuvable.~~ **~~in a 2-D axisymmetric computational domain.~~** The flow velocities are very low and decrease during the formation of the cake as the latter creates hydraulic resistance to

the flow. These velocities are in the order of 10^{-5} m·s^{-1} at t = 1.5 h, which is in agreement with a Stokes-type laminar flow **[20]**. PSC kinetics obtained by the numerical model are in very good agreement with the experimental measured values of cake thickness as exposed in Figure 4b. For example, after 24 h of PSC under a constant pressure of $3 \cdot 10^6$ Pa, the pieces are approximately 110 mm thick, which was predicted by the simulator in the same conditions. **The simulation** reveals, among other things, that the casting conditions, under a 3 MPa pressure, are of the kind expected to lead to cakes exhibiting a high sinterability: (i) lack of turbulence during suspension flow, despite the significant pressure applied; (ii) uniformity of pressure distribution over the mould surface; and (iii) gradual building up of the cake **[20]**.

3.1.2 Comparison of PSC with other forming methods

For allowing comparison of sinterability, YAG-based ceramics were shaped by PSC, SC and CIP. At first, the bulk density of the green-compacts (BD_g) was measured and results are given in Table 1. The entire thickness (*i.e.* 5-10 mm) of YAG discs was analyzed (samples S1 to S4) whereas for the rod different sections of 10 mm in length were cut (samples S5a to S5c).

Table 1: Green density, pore size distribution and optical transmittance of YAG specimens (YAG-P1 and YAG-P2 ; discs S1-S4 and a rod S5 of 85 mm in length), as a function of forming and sintering method.

Sample number (position)	Type of powder	Forming Method (Pressure in MPa)	BDg (g·cm^{-3})	% TD (%)	PoSD mode (nm)	Sintering conditions	RIT_{max} (%)
S1 (disc)	YAG-P1	CIP (120)	2.54	55.8	-	AS+HIP	63[(a)]
S2 (disc)	YAG-P1	PSC (2)	2.63	58.0	70	AS+HIP	78[(a)]
S3 (disc)	YAG-P2	SC	1.84	40.5	86	VS	53[(b)]
S4 (disc)	YAG-P2	PSC (3)	2.46	54.1	70	VS	84[(b)]
S5a (rod) (0-	YAG-P2	PSC (3)	2.44	53.7	63	VS	74[(b)]

10 mm)							
S5b (rod) (30-40 mm)	YAG-P2	PSC (3)	2.46	54.1	63	VS	75[(b)]
S5c (rod) (70-80 mm)	YAG-P2	PSC (3)	2.47	53.7	63	VS	78[(b)]
S6 (disc)	YAG-P2	CIP (100)	2.17	51.8	85	-	-

[(a)] t = 2 mm, λ = 700 nm.
[(b)] t = 5 mm, λ = 700 nm.

Second, the pore size distribution of green specimens, formed by respectively SC (S3), PSC (S5a-c) and CIP (S6), is presented in Figure 5b. One can see that both the green density (compacity) and pore size distribution are very homogeneous all along the rod. The compacity remains close to 54±0.5% whatever the analyzed section of the rod from 0-10 mm to 70-80 mm.

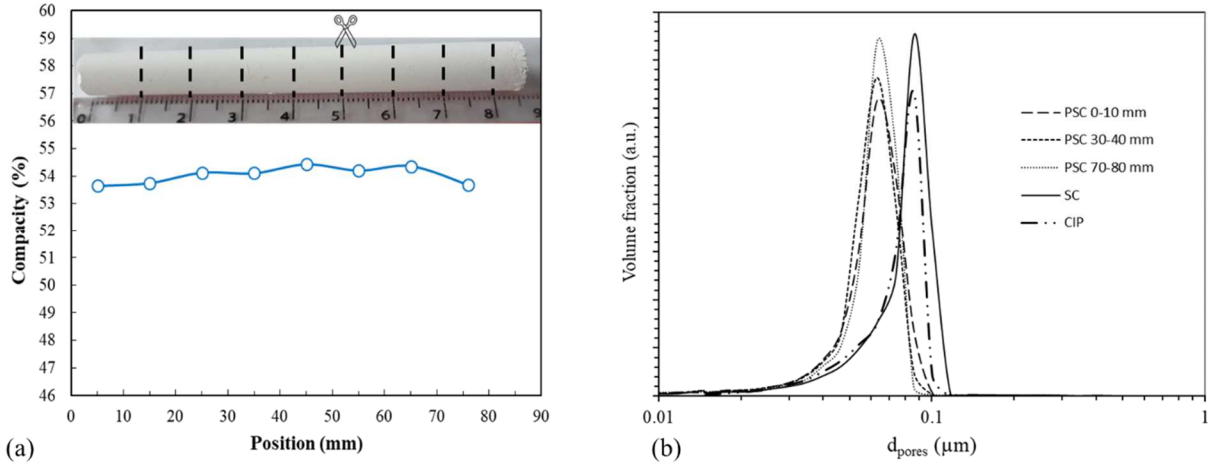

*Figure 5: Compacity along a rod of YAG of 85 mm in length by 10 mm in diameter obtained by PSC **(sample S5)** and corresponding view (a). Comparison of the pore size distribution (Hg intrusion measurement) of YAG green compacts formed by PSC **(S5a-c)**, SC **(S3)** and CIP **(S6)**. The positions (XX-YY mm) refer to the analyzed section of the rod illustrated in (a).*

As it can be seen, in the Figure 5b and Table 1, both the pore size distribution and the green-density exhibit, in the case of PSC, values more suitable than SC and CIP if sinterability of the formed parts is of interest. Dilatometry analyses were performed on green parts derived

from powder YAG-P2 shaped by these different forming methods. From the measured shrinkage $\Delta L_{(T)}/L_0$, the relative density was calculated according to Eq. (3):

$$\rho_{(T)} = \frac{\rho_0}{\left(1 - \frac{\Delta L_{(T)}}{L_0}\right)^3} \qquad \text{Eq. (3)}$$

where $\rho_{(T)}$ is the relative density at a given temperature T and ρ_0 the initial relative density of the green compact. By considering that there is no mass loss or structural change in the samples for temperatures above 1450°C (*i.e.* after YAG phase formation [31]), such approach gives a good approximation of the evolution of the relative density of YAG ceramics during thermal treatment, *i.e.* sinterability can be discussed based on these results. As exposed in Figure 6, the obtained curves have a classical shape when densification is the predominant sintering mechanism. All samples were fully dense after sintering with $\rho > 99\%$ whatever the shaping technique used. It is clear from these results that the densification of PSC sample occurs at lower temperature. PSC sample reaches 90% of relative density at 1600°C when it increases to 1640°C for CIP and 1655°C for SC. Such result confirms that the pore size distribution plays a major role on green compact ability to densify.

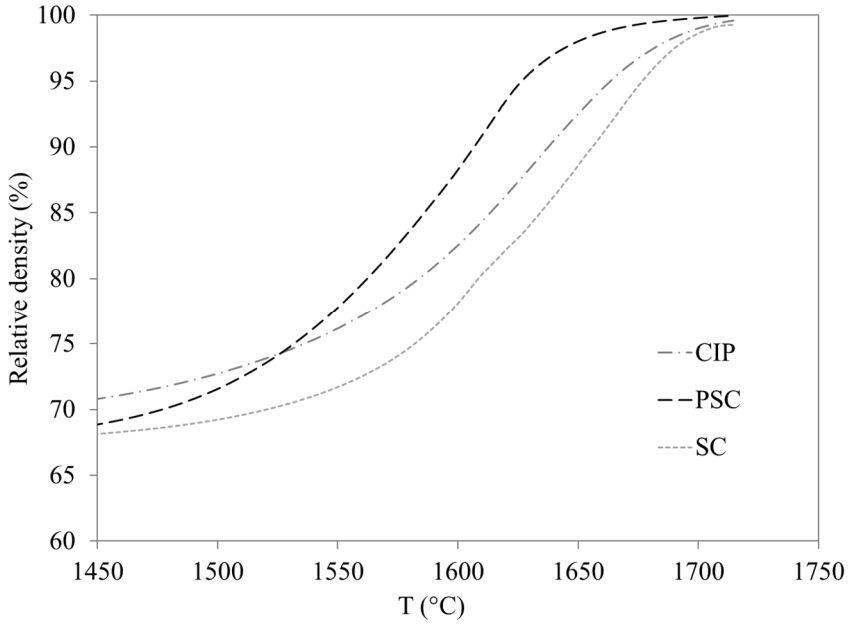

*Figure 6: Relative density as a function of temperature obtained by dilatometry. Sintering was conducted under vacuum for YAG green compacts (YAG-P2) formed by PSC **(S4)**, SC **(S3)** or CIP **(S6)**.*

Finally, specimens derived from powder YAG-P2 were vacuum fired to achieve transparency and corresponding pictures were presented in Figure 7a-c. Their optical transmission was then measured. Typical transmission curves, generated by such specimens, are shown in Figure 7d. The maximal RIT levels (at λ = 700 nm) are also presented in Table 1.

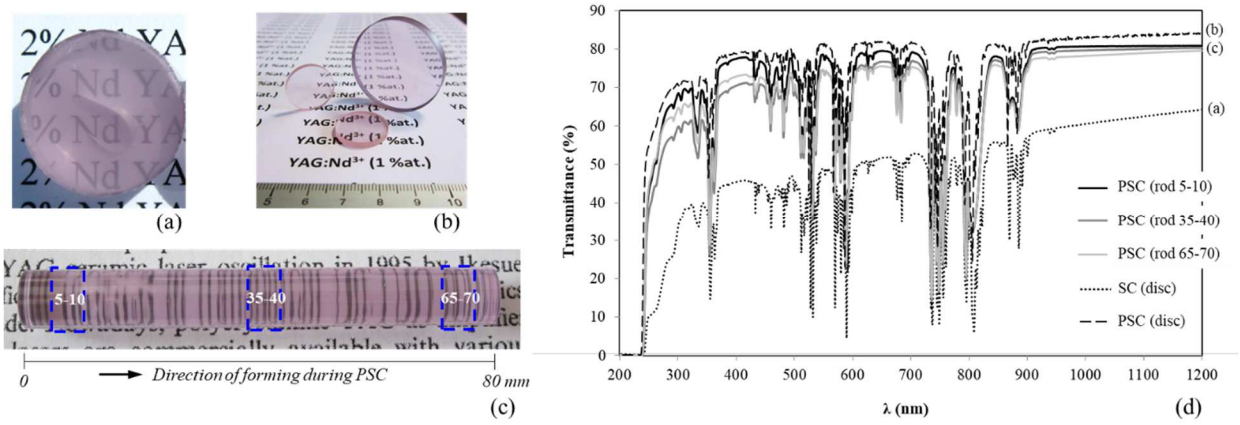

*Figure 7: Pictures of 1at.%Nd:YAG ceramics from YAG-P2 powder after VS shaped by SC (**sample S3:** 25 mm in diameter, 5 mm thick) (a) or PSC in the form of discs (**sample S4:** 40 mm in diameter, 5 mm thick) (b) or rod (**sample S5:** 10 mm in diameter, 80 mm in length) (c) and corresponding optical transmission spectra (d). Analyzed zones of the rod were indicated in dotted lines with corresponding position.*

As it can be seen a higher level of transmission was achieved for PSCed samples. The S4 disc attained the theoretical value (*i.e.* 84% at a wavelength of 700 nm). Sample obtained by SC has the lowest transmission baseline indicating that a lot of light is scattered by residual defects, in accordance with the fuzzy aspect of the text behind the sample in Figure 7a. On the other hand PSC, which ensures a similar pore size distribution and low average pores size over all the volume of the specimens (even for the largest rod) generates parts in which the high transmission level is maintained over the whole length of the rod shaped sample. It is worth to notice here that such rod, with a length of 110 mm in the green state and 80 mm after

sintering, was obtained by longitudinal filtration, *i.e.* only through one side of the rod as illustrated in Figure 7c. Such a high thickness was obtained thanks not only to an appropriate optimization of the stability of the suspensions, but also to an optimization of the PSC apparatus and its control parameters. In fact, obtaining a rod of 110 mm in length prior to sintering, is not trivial and takes at least 24 h under a constant pressure of 3 MPa according to the results presented in the section 3.1.1 (see Figure 4b).

According to optical microscopy analyses reported in Figure 8, defects are mainly residual porosity with different morphological characteristics depending on the shaping technique used. For liquid forming methods, *i.e.* SC and PSC, the residual porosity appears to be well distributed throughout the sample and the average pore size is quite small with the largest pore diameter not exceeding a few micrometers. As expected from visual inspection and optical transmission measurements reported in Figure 7, SC sample shows much more residual pores than PSC sample. For solid-way forming technique, *i.e.* CIP, the size distribution of residual pores appears much more heterogeneous with some large pores exceeding 50 µm. The occurrence of these large pores and its implication on sintering and optical properties will be discussed in the last section of this study.

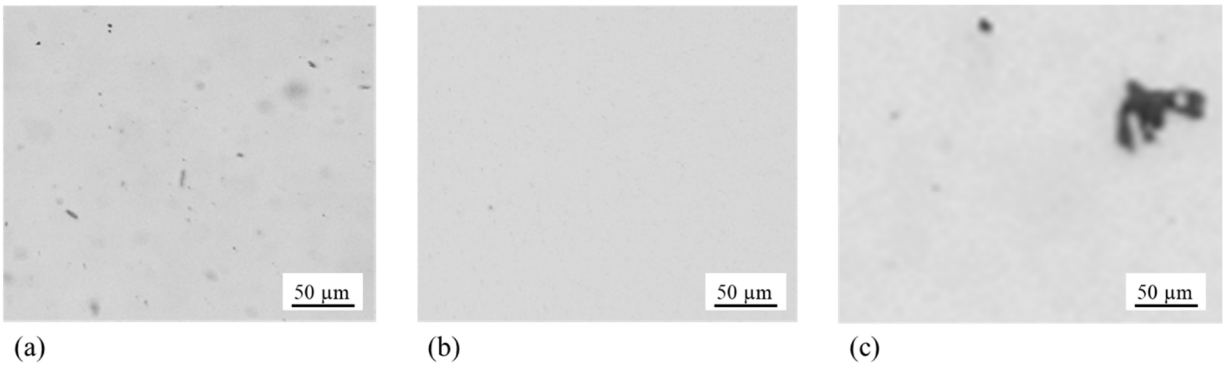

*Figure 8: Micrographs obtained by optical microscopy of 1at.%Nd:YAG ceramics from YAG-P2 powder after VS shaped by SC **(sample S3)** (a), PSC **(sample S4)** (b) or CIP **(sample S6)** (c). Residual porosity appears as black spots.*

3.1.3 Study of sintering by air + post-HIP

Before proceeding, let us note that a firing procedure-in which the standard long vacuum firing is replaced by a sinter **(in air)**/post-HIP method constitutes an approach which may be interesting, when industrial manufacturing is envisaged, mainly because it requires a furnace type significantly less costly than a vacuum furnace. Thus, processing by sinter(air)/HIP, despite the two sintering stages included, could be advantageous compared to long vacuum firing. Owing to the above a preliminary examination of such an approach was effectuated before this research. In that preliminary work, CIPed discs were sintered in air at 1720°C for 3 h (BD_f = 4.41 $g.cm^{-3}$; OP = 0.4%) and then post-HIPed at 1800°C. In these conditions, the specimens obtained after HIP could not be brought to transmission levels higher than 40-45 % (λ = 700 nm, t = 2 mm), owing to the unsatisfactory microstructure of the green bodies. The improved quality of the green bodies, achieved in this work, especially by PSC, suggested that the air sintering based densification process might give better results now. Thus, it was decided to test again here the sinter(air)/HIP firing approach.

In this part of the study, both PSC and CIP formed discs derived from YAG-P1 powder were used. At first, suitable microstructure of pre-sintered samples before HIP must be obtained, *i.e.* the open porosity should be lower than 1% and the relative density higher than 96%. The results, in terms of bulk density (BD_f) and open porosity (OP) values as a function of air sintering temperature are given in Table 2.

Table 2: Bulk density (BD_f), theoretical density (TD) and open porosity (OP) of air sintered YAG specimens at Ts = 1630°C,1680°C, 1710°C and 1750°C as a function of forming procedure.

Sample number	Type of powder	Forming method	Ts (°C)	BD_f ($g \cdot cm^{-3}$)	% TD (%)	% OP (%)
S1a	YAG-P1	CIP	1680	4.46	98.0	0.1
S1b	YAG-P1	CIP	1710	4.43	97.4	0.4
S1c	YAG-P1	CIP	1750	4.38	96.3	0.7
S2a	YAG-P1	PSC	1630	4.40	96.7	0.8

S2b	YAG-P1	PSC	1680	4.51	99.1	0.05
S2c	YAG-P1	PSC	1710	4.48	98.5	0.15
S2d	YAG-P1	PSC	1750	4.40	96.7	0.8

A first observation suggested by the data in the Table 2 was that in the case of air-sintering, as opposed to VS, using excessive temperatures is deleterious not only to the furnace but also to the densification process itself. The values show that 1680°C is optimal for YAG sintering in air whatever the forming method, when the microstructure of the green-bodies is adequate. While bulk-density levels rise up to 1680°C, at higher temperatures they are degraded. This is, probably, a consequence of exaggerated grain growth generally encountered at excessive sintering temperatures, especially in YAG [31], and/or the gas pressure developed in the closed pores (not happening during vacuum firing); over a certain temperature it gets high enough to oppose densification [32]. It is also seen that the BD_f of discs formed by PSC is higher than that of the pressed ones. However, the most important result, shown in Table 2, is the possibility to densify specimens to a low level of open porosity (lower than 0.5%) – very convenient to further HIPing – at temperatures accessible to furnaces operating in air.

In Figure 9 the optical transmission of parts formed by CIPing and respectively PSC and then densified by sinter(air)/HIPing are shown. The RIT values, at λ = 700 nm, are presented also in Table 1. The first sintering step in air was done as recommended by Table 2 at 1680°C for 4 h while the closing of the residual porosity was performed by HIPing at 1800°C.

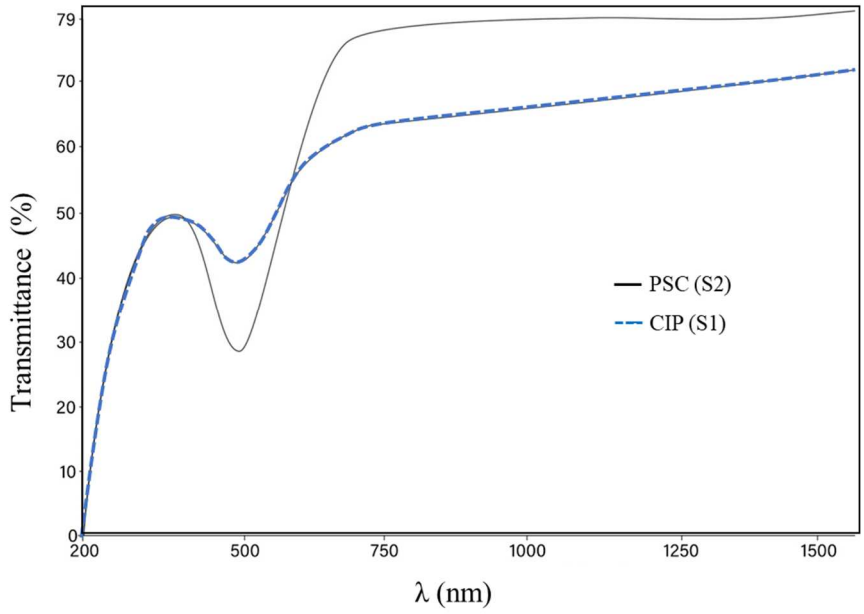

Figure 9: Transmission of YAG specimens derived from powder YAG-P1 and densified by a sinter(AS)/post-HIP approach (absorption band at 500 nm introduced by Y^{2+} see text). Top curve: green-bodies formed by PSC, lower curve: green-bodies formed by CIPing.

As Figure 9 shows, the transmission of the disc formed by PSC (and sinter(air)/post-HIP) is some 16% higher (at λ = 700 nm) than that of the specimen compacted by CIP and densified in the same way. The absorption band, located at ~ 500 nm (Figure 9) is owed to the partial reduction of Y^{3+} to Y^{2+} during HIPing (if Si is present as sintering aid, as explained in [22,33]). Its elimination requires a long annealing in air, around 1400°C. The reduction of Y^{3+} occurs also during vacuum firings but when these exceed 15 hour dwells at T > 1750°C, its intensity is very much reduced, probably owing to Si exit from the YAG lattice. The BD_g of the PSCed specimen is here higher than that of the CIPed one. Comparing the transmission, ensured by the PSCed specimen subjected to sinter(air)/HIPing, to similar ones densified by vacuum firing (curves “a” and “b”, in panel d of Figure 7), it is seen that the former is lower. Nevertheless, YAG primary powders were not the same and additional experiments are needed to determine the critical parameter leading to such difference (YAG primary powders

and/or processing). Thus, further increasing the transmission of air sintered specimens, by powder choice and/or processing refining of the sinter/HIP approach, seems feasible.

3.2. Spinel ceramics

In the case of spinel also the results produced by SC, PSC and CIP methods were examined. The green-state bulk density (BD_g) of discs, formed by all the three forming methods considered, is listed in Table 3, in terms of theoretical density (TD) percentage. For spinel the TD = 3.578 $g \cdot cm^{-1}$. In addition, Table 3 also conveys the sintering conditions (first sintering stage by AS) required to bring each powder type to a densification level of 97% TD. The transparency level attained after the sinter/HIP stage (for spinel only the air sinter/post-HIP densification approach was used) is also given in Table 3. From previous experience we know that such a density is the minimal one at which the open porosity is near-fully closed (see also Table 2, regarding YAG were the issue also came up) [7].

Table 3: Green state characteristics, pores closing firing temperature (3 h dwell) and dense parts optical transmission (RIT) as a function of forming procedure.

Sample number	Forming method	BD_g (%)	% TD (%)	P_oSD mode (nm)	Ts for BD_f = 97%[(a)] (°C)	RIT_{max}[(b)] (%)
S7	SC	1.72	48	85	1550	Translucent
S8	PSC	2.00	56	43	1480	84
S9	CIP	1.82	51	55	1480	79

[(a)] 3 h of dwell time at sintering temperature Ts.
[(b)] t = 1 mm, λ = 700 nm.

In Figure 10 the pore size distribution of parts considered in Table 3 are presented. One can see that the pore size distribution of spinel-based green compacts lies in similar domain (*i.e.* 0.02-0.2 μm) than that observed previously for YAG in Figure 5b. This owing to the similar forming method used. The P_oSD mode obtained by using PSC (*i.e.* 43 nm) is significantly lower than that obtained by CIP (*i.e.* 55 nm) and SC (*i.e.* 85 nm). This result once again

highlights the greater ability of PSC to produce green compacts probably having a greater sinterability.

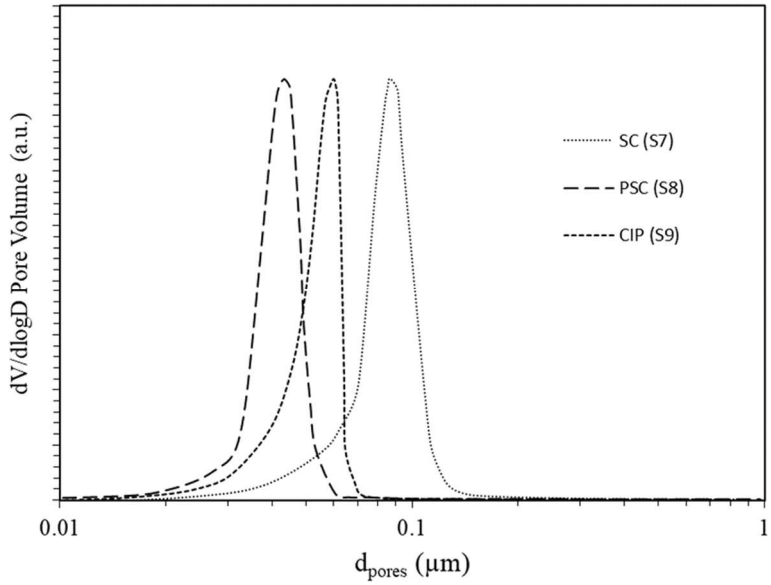

Figure 10: Pore size distribution of spinel green-discs formed by various methods. Forming by SC (sample S7), PSC (sample S8) and CIP (sample S9).

In Figure 11 the optical transmission spectra of sintered discs formed respectively by CIP and PSC are given. ~~**For the case of CIPed parts, two analyzed samples are considered in this Figure: one typical for exhibiting maximal transmission (samples 9A, RIT = 81% at 700 nm, 80% at 400 nm) and one for those having minimal transparency (sample 9B, RIT = 79% at 700 nm, 66% at 400 nm).**~~

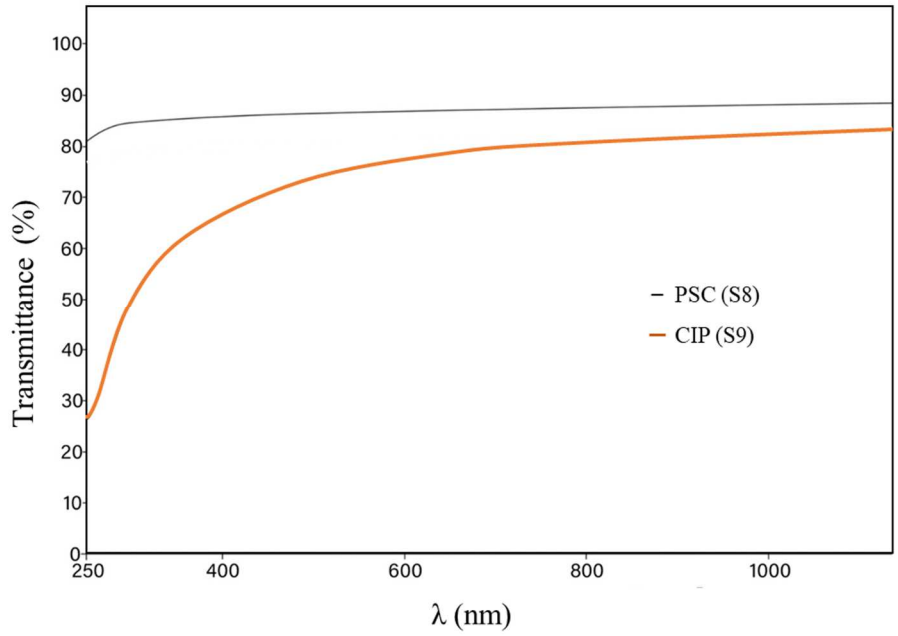

Figure 11: Transmission of spinel specimens formed by PSC ***(sample S8)*** *and CIP* ***(sample S9)*** *(t = 1 mm).*

The optical transmission of the PSCed disc **(sample S8)** is around 84% at 700 nm. For **the sample S9** made by CIP, the RIT reaches some 80% at 700 nm ~~**and a bit lower for the sample 9B**~~. However, importantly, the latter curve drops significantly under 550 nm, corresponding to a significantly lower overall transparency. The transmission drop occurs in the wavelength region where incident light intensity loss, owed to scattering, is supposed to be strong [1]. The Figure 12 shows micrographs obtained by optical microscopy in transmission mode of spinel samples obtained by various shaping techniques (*i.e.* SC, PSC and CIP for S7, S8 and S9, respectively). Typical variants regarding morphology, size and pores clustering pattern are illustrated. The opaque zones, which constitute the main defect affecting light transmission by the scattering they cause, can be attributed to pores or pores agglomerates. Significant differences are revealed by these analyses and it is clear that PSC forming technique favor microstructural homogeneity and less pore agglomerates in sintered parts.

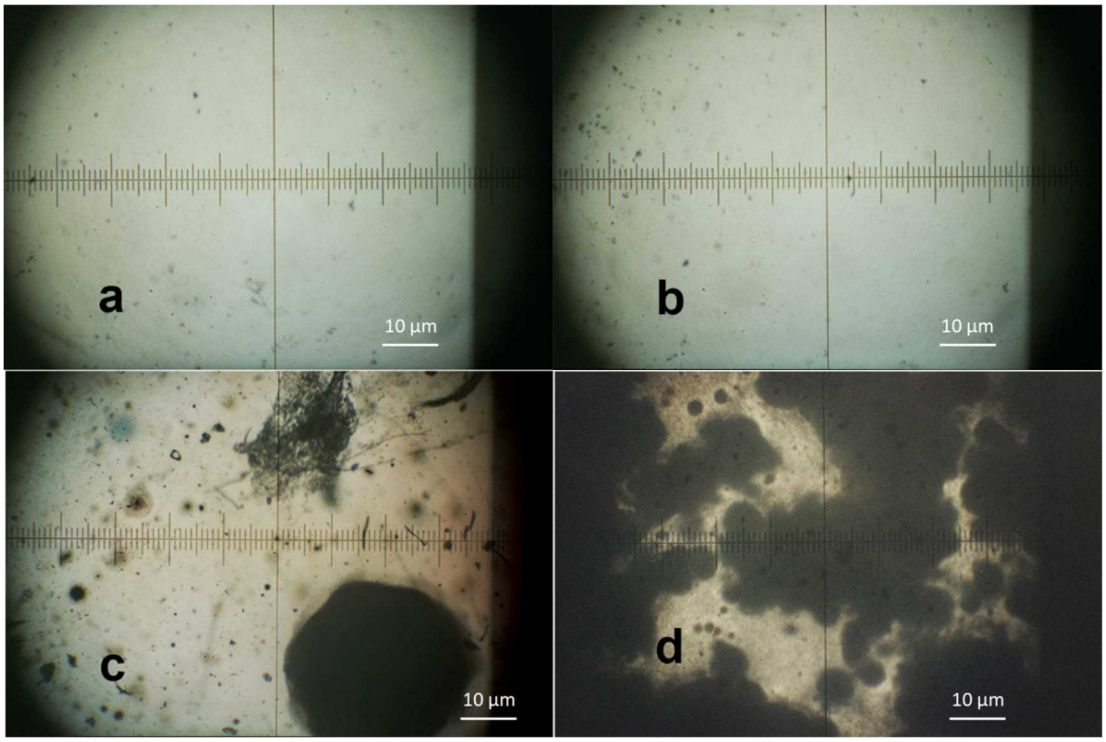

Figure 12: Some typical types of defect (size, morphology and distribution patterns shown) encountered in the spinel specimens formed by PSC ***– sample S8*** *(a, b), CIP* ***– sample S9*** *(c) and SC –* ***sample S7*** *(d).*

Comparison of the data carried by Figures 9-11 and Table 3 allows one to establish some interesting correlations between green-body features and sintered discs transparency. **It is useful to recall here that always the same raw Spinel powder was used. Only milling and shaping processes were modified. Therefore, the obtained results are the consequence of the sintering of the same nanoparticles, and the differences observed only come from a different ratio between agglomerates and dispersed particles. In green compacts, such differences can be measured by the pore size distribution. In sintered samples, optical micrographs reported in Figure 12 show a transparent matrix containing more or less isolated pores or pore clusters depending on the process used. That means Spinel nanoparticles globally sinter to full densification, at the condition that pores in green compacts is not too big, *i.e.* there is not too big and hard agglomerates in the shaped powder. As an example,** the individual pores size is not very different between discs shaped

by PSC and CIP (see Figure 10). In consequence, specimens formed by the two methods do not differ markedly in transparency (see Figure 11) as long as the majority of remnant pores are **sufficiently small and well dispersed for the two samples**. The differences are, as optical microscopy reveals, a consequence of the pores clustering patterns which are more often encountered in CIPed parts. In fact, the examination of numerous zones of sintered samples by optical microscopy revealed that for PSC formed specimens, Figure 12a,b is representative of the type and distribution of defects encountered in the whole volume of the specimen. In the CIP formed disc, dense and transparent zones coexist with scattered defect-rich zones (pore agglomerates) as illustrated in Figure 12c **for sample S9**. ~~**The latter explain the discrepancy of transmission values obtained for CIPed samples (samples S9A and S9B).**~~ The pattern seen in Figure 12d was visible only in the milky discs formed by simple slip-casting **(sample S7)**, where pore agglomerates appeared with quite high frequency.

The data discussed above suggest that by CIPing and pressure casting specimens exhibiting quite similar maximal transmission levels are achievable. This is consistent with the quite small difference in the pores size average and distribution width of the green bodies of the compared specimens. The SCed specimens have significantly higher average pore size than that exhibited by PSCed and even the CIPed discs. This makes their full and uniform densification not feasible precluding attainment of high levels of transparency (some translucency is the best result one may achieve). Related to this discussion it seems useful to recall, from the literature, the fact that from a powder based on nano-size spheroidal particles (*e.g.* prepared by flame spray pyrolysis) quite high transparency (T = 50 % at λ = 600 nm; t = 2 mm) could be achieved by simple air sintering at temperatures as low as 1350°C; and by HIPing at a similar temperature transmission rose to 81% [7]. This could be achieved because that powder, while producing agglomerates similar **to those observed in this study**, had certain specific features that enabled one to form, by CIPing, green-bodies having an average

pores size not larger than 25 nm. This example further highlights the conclusion regarding the critical influence of a uniform small pores size (throughout the specimen`s volume), conditioned not only by the morphological characteristics of the powder but also by the forming method, as suggested by the findings of this work.

Finally, spinel transparent ceramics with large size were successfully manufactured by PSC at industrial level by PSC as illustrated in Figure 13. Samples were as large as 150x150x20 mm with homogeneous and good level of transparency.

Figure 13: Example of large spinel pieces (150x150x20 mm for the largest) produced by PSC after sintering and polishing.

4. Discussion

The data presented by the previous sections suggest that PSC is the forming approach generating the most sinterable green-parts, both in the case of YAG and spinel. An interesting consequence is that, owing to the sinterable powder compacts it generates, PSC allows the employment of air pre-sintering as the first step in a two-step densification approach using post-HIP as the final densification treatment. Based on these observations, one can discuss the critical role of initial pore size distribution on the sintering behaviour of green compacts. In fact, in the case of transparent ceramics, the manufacturing process must lead to a

concentration of microstructural defects (pores, inclusions of secondary phases, etc.) extremely low. To this end, each of the steps in the process must aim to promote purity, microstructural homogeneity and final density (and thus the elimination of residual porosity) of such ceramics. The kinetics of elimination of the residual pores - which constitute the main microstructural defects responsible for the deterioration of transparency - is closely dependent on their size. In particular, a distribution in poly-dispersed pore size (*i.e.* admitting several populations of distinct mean sizes) can lead to differential sintering and, ultimately, partial elimination of the porosity. Owing to their size, the densification kinetics of large pores can be too low to lead to full densification at the end of sintering, even under pressure-assisted sintering like post-HIP. These phenomena were well illustrated by Krell *et al.* in their studies on transparent ceramics manufacturing [5,6]. Their works and those reported here show that the shaping process strongly influences the reactivity to the sintering of the granular compact. The experience also shows that it is difficult to synthesize isolated and poorly aggregated ceramic particles, especially when they are fine (submicrometric), even very fine (nanometric). Interactions between particles are also becoming stronger when their size decreases, which does not favor their reorganization during the granular compact shaping step. Thus, the homogeneity of granular compacts tends to decrease with the radius of the particles that compose it. Finally, it allows or not the total elimination of the porosity at the end of sintering.

For this reason, it is essential to work in a first time on the synthesis processes of pure, reactive and homogeneous powders and then on shaping processes especially optimized to avoid the generation of any microstructural defects in the parts before sintering. It is useful to mention here that the reactivity at sintering is not the same for an isolated powder particle than for a more or less compact set of these same particles: (1) for an isolated particle, its reactivity increases with the decrease in its radius due to the increase in curvature and the

reduction of characteristic diffusion distances. In other words, the sintering temperature decreases with particle size; (2) for a set of particles, the reactivity is also a function of its homogeneity which tends to increase the temperature sintering when it degrades. This phenomenon is explained essentially by the differential densification observed between the zones of high compactness (agglomerates or aggregates) and those of lower compactness (inter-agglomerated zones) as illustrated in Figure 14(a) A [34]. According to this scheme, a perfectly homogeneous green compact should have only one type of pores, denoted pores of type I, with fine and narrow size distribution. In the case of an agglomerated and/or aggregated powder synthesized by a given chemical route, aggregates have generally a finer pore size, denoted pores of type IIa. Moreover, these aggregates tend to form voids, denoted pores of type IIb, when they are compacted due to poor rearrangement ability during packing. As a result, even few aggregates can lead to microstructural heterogeneities in the green compacts that can lead to differential sintering during thermal treatment as illustrated in Figure 14(a) B-D. In such case, aggregates should sinter before the rest of the matrix leading locally to coarser microstructure and pores of type IIb should lead to residual porosity at the end of sintering owing to slow densification kinetics. Also, the regions that densify faster (*i.e.* aggregates in this case) exert tensile stresses on the neighboring regions that are densifying more slowly. As a result, pores of type IIb can grow rather than shrink during the intermediate stage of densification (step B in Figure 14(a)), despite the fact that the compact undergoes an overall shrinkage [34].

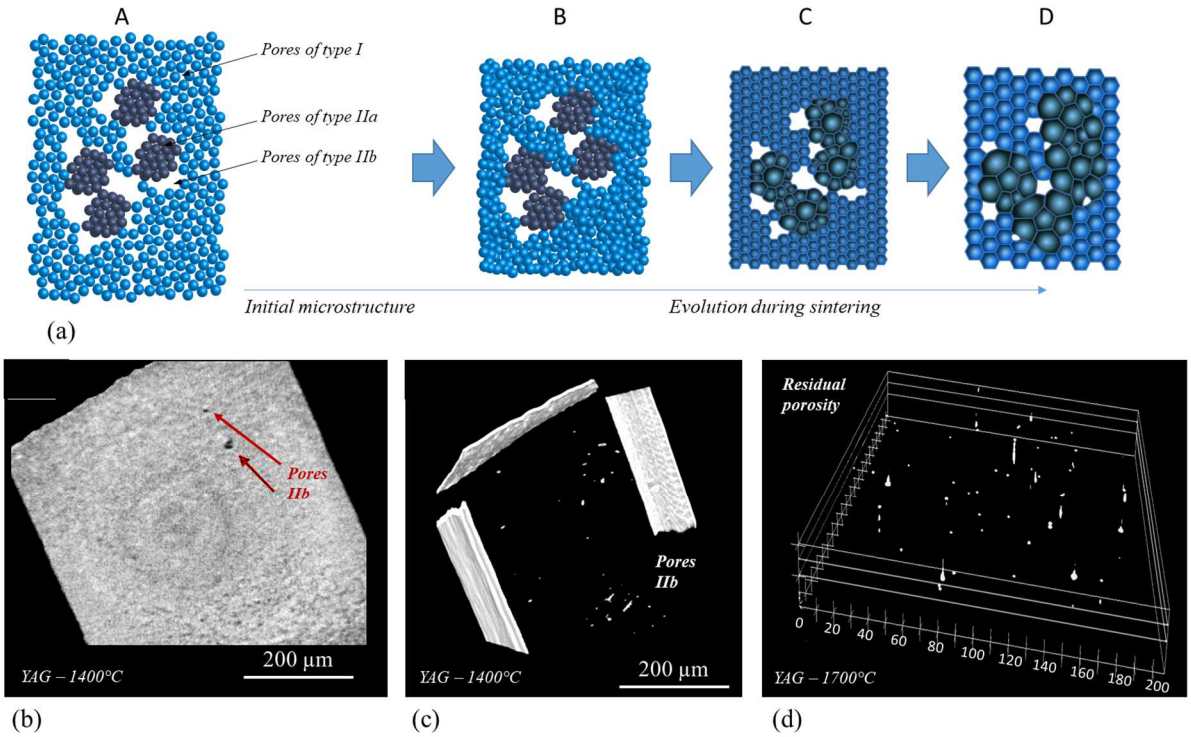

*Figure 14: Microstructure evolution model for the densification of different types of pores: green part (A), pore densification of smaller size (type I and IIa) at low temperature accompanied by moderate grain growth (B and C), densification of the larger pores (type IIb) (D) which become unstable under the effect of rapid granular growth at high temperature (a). X-ray microtomography micrograph showing large pores of type IIb in a YAG sample shaped by PSC **(sample S4)** and vacuum-fired at 1400°C (i.e. at intermediate stage of sintering, ρ = 75%), 2D cut in (b) and 3D view after segmentation in (c). Confocal laser scanning microscopy showing residual porosity in 3D in transparent YAG sample shaped by PSC **(sample S4)** and vacuum-fired at 1700°C (i.e. at final stage of sintering, ρ > 99.9%).*

For transparent ceramics manufacturing, the difficulty lies in the detection and quantification of the defects for very low levels (<1% vol.), whatever the type of microstructural defect concerned (*i.e.* porosity, secondary phases, etc.). As an example, a porosity of 0.001% (10ppm vol.) consisting of pores of 300 nm in diameter limits the transparency of YAG ceramics to a value of around 60-70% [25,35]. Analytical techniques suitable for detecting defects in this case rely for the most part on optical (for transparent pieces), X-ray or electron microscopy, possibly in three dimensions, which allows a larger sample volume to be analyzed thus increasing the reliability and easiness of defects detection. Figure 14(b-d) illustrates the evolution of defects in YAG ceramics along the thermal treatment. Pores of

type IIb were easily detected by X-ray microtomography as illustrated in Figure 14(b and c) in YAG samples fired under vacuum at 1400°C, *i.e.* at the intermediate stage of densification (ρ = 75%). The mean diameter of these pores was around 2 µm and their volume density is in the order of $2 \cdot 10^{7}.cm^{-3}$, corresponding to a very low porosity of 8.10^{-3}%. At this step of the process, such volume represents only 10^{-4}% of the total porosity in the ceramic part illustrating that making transparent ceramics needs almost "zero" defects. After full densification at 1700°C, similar values for porosity characteristics are obtained when the obtained sample was examined by confocal laser scanning microscopy as illustrated in Figure 14(d). So, residual porosity should mainly come from these defects of type IIb in transparent part. These results clearly illustrate the previous described schemes and pave the way for fully transparent ceramics manufacturing. Finally, the PSC shaping process, owing to its ability to produce green compacts with homogeneous and fine porosity in the case of using "good" raw powders, is a very good candidate for transparent ceramics manufacturing.

5. Conclusions

This study has shown that pressure slip casting (PSC) is able to generate, both in the case of spinel and YAG, green bodies exhibiting a fine, uniform porosity and high bulk density, even for large size pieces. As a result such parts exhibit the high sinterability required by transparent products fabrication. PSC appears as a method of forming green ceramics parts with less microstructural defects (*i.e.* large pores and/or pore clusters), than conventional slip casting or cold isostatic pressing**, independently of the morphological or chemical characteristics of the powder.** As a result, highly transparent spinel and YAG ceramics with large size suitable for many applications like high power laser amplifier media or transparent armor were produced.

Acknowledgments

Part of this work was funded by the French Agency DGA through the RAPID - CERAGRAD project under grant Nb. 152906083. **This work was also supported by institutional grants from the National Research Agency under the Investments for the future program with the reference ANR-10-LABX-0074-01 Sigma-LIM.** The authors are also grateful to Ali Chirazi (ICMCB, Bordeaux, France) for X-ray microtomography measurements.

References

[1] A. Goldstein, A. Krell, Z. Burshtein, Transparent Ceramics: Materials, Engineering, and Applications, John Wiley & Sons, NY, 2020.
[2] A. Goldstein, A. Krell, Transparent Ceramics at 50: Progress Made and Further Prospects, J. Am. Ceram. Soc. 99 (2016) 3173–3197. https://doi.org/10.1111/jace.14553.
[3] A. Ikesue, Y.L. Aung, V. Lupei, Ceramic Lasers, 1 edition, Cambridge University Press, Cambridge, 2013.
[4] A. Goldstein, Correlation between MgAl2O4-spinel structure, processing factors and functional properties of transparent parts (progress review), J. Eur. Ceram. Soc. 32 (2012) 2869–2886. https://doi.org/10.1016/j.jeurceramsoc.2012.02.051.
[5] A. Krell, T. Hutzler, J. Klimke, Transmission physics and consequences for materials selection, manufacturing, and applications, J Eur Ceram Soc. 29 (2009) 207–221. https://doi.org/10.1016/j.jeurceramsoc.2008.03.025.
[6] A. Krell, J. Klimke, Effects of the Homogeneity of Particle Coordination on Solid-State Sintering of Transparent Alumina, J Am Ceram Soc. 89 (2006) 1985–1992.
[7] A. Goldstein, A. Goldenberg, M. Vulfson, Development of a Technology for the Obtainment of Fine Grain Size, Transparent MgAl2O4 Spinel Parts, J. Ceram. Sci. Technol. 2 (2011) 1–8. https://doi.org/10.4416/JCST2010-00018.
[8] F.F. Lange, Powder Processing Science and Technology for Increased Reliability, J. Am. Ceram. Soc. 72 (1989) 3–15. https://doi.org/10.1111/j.1151-2916.1989.tb05945.x.
[9] A. Roosen, H.K. Bowen, Influence of Various Consolidation Techniques on the Green Microstructure and Sintering Behavior of Alumina Powders, J. Am. Ceram. Soc. 71 (1988) 970–977. https://doi.org/10.1111/j.1151-2916.1988.tb07567.x.
[10] J.S. Reed, Principles of Ceramics Processing, 2nd Edition, 2 edition, Wiley-Interscience, New York, 1995.
[11] J.A. Lewis, Colloidal Processing of Ceramics, J. Am. Ceram. Soc. 83 (2000) 2341–2359. https://doi.org/10.1111/j.1151-2916.2000.tb01560.x.
[12] R.E. Fouts, R.P. Johnston, Pressure slip casting process for making hollow-shaped ceramics, 5 427 722, n.d. http://www.google.com/patents/US5427722 (accessed October 11, 2015).
[13] Richter, H.J., Pressure slip casting of silicon nitride, in: Ceram. Process. Sci. Technol. Proc. Fifth Int. Conf. Ceram. Process. Sci. Technol., Westerville, 1995: pp. 439–443.
[14] T.J. Fennelly, J.S. Reed, Mechanics of Pressure Slip Casting, J. Am. Ceram. Soc. 55 (1972) 264–268. https://doi.org/10.1111/j.1151-2916.1972.tb11277.x.

[15] J.M.F. Ferreira, H.M.M. Diz, Effect of ageing time on pressure slip casting of silicon carbide bodies, J. Eur. Ceram. Soc. 17 (1997) 333–337. https://doi.org/10.1016/S0955-2219(96)00110-0.
[16] J.H.D. Hampton, S.B. Savage, R. a. L. Drew, Experimental Analysis and Modeling of Slip Casting, J. Am. Ceram. Soc. 71 (1988) 1040–1045. https://doi.org/10.1111/j.1151-2916.1988.tb05789.x.
[17] J.B. Hurst, S. Dutta, Simple Processing Method for High-Strength Silicon Carbide, J. Am. Ceram. Soc. 70 (1987) C-303-C-308. https://doi.org/10.1111/j.1151-2916.1987.tb05642.x.
[18] E.G. Blanchard, Pressure casting improves productivity, Am. Ceram. Soc. Bull. 67 (1988) 1680–1683.
[19] R. Moreno, A. Salomoni, I. Stamenkovic, S.M. Castanho, Colloidal Filtration of Silicon Nitride Aqueous Slips, Part II: Slip Casting and Pressure Casting Performance, J. Eur. Ceram. Soc. 19 (1999) 49–59. https://doi.org/10.1016/S0955-2219(98)00137-X.
[20] R. Boulesteix, C. Chevarin, R. Belon, A. Maître, L. Cochain, C. Sallé, Manufacturing of Large Size and Highly Transparent Nd:YAG Ceramics by Pressure Slip-Casting and Post-Sintering by HIP: An Experimental and Simulation Study, Materials. 13 (2020) 2199. https://doi.org/10.3390/ma13092199.
[21] Yu.L. Kopylov, V.B. Kravchenko, S.N. Bagayev, V.V. Shemet, A.A. Komarov, O.V. Karban, A.A. Kaminskii, Development of Nd3+:Y3Al5O12 laser ceramics by high-pressure colloidal slip-casting (HPCSC) method, Opt Mater. 31 (2009) 707–710.
[22] A. Goldstein, Alexander.I. Shames, A.J. Stevenson, Z. Cohen, M. Vulfson, Parasitic Light Absorption Processes in Transparent Polycrystalline MgAl2O4 and YAG, J. Am. Ceram. Soc. 96 (2013) 3523–3529. https://doi.org/10.1111/jace.12525.
[23] A. Goldstein, A. Goldenberg, M. Hefetz, Transparent polycrystalline MgAl2O4 spinel with submicron grains by low temperature sintering, J Ceram Soc Jap. 117 (2009) 1281–1283.
[24] A. Krell, P. Blank, The Influence of shaping method on the grain size dependence of strength in dense submicrometre alumina, J. Eur. Ceram. Soc. 16 (1996) 1189–1200. https://doi.org/10.1016/0955-2219(96)00044-1.
[25] R. Boulesteix, A. Maître, J.-F. Baumard, Y. Rabinovitch, Quantitative characterization of pores in transparent ceramics by coupling electron microscopy and confocal laser scanning microscopy, Mater Lett. 64 (2010) 1854–1857.
[26] E.A. Borisova, P.M. Adler, Deposition in porous media and clogging on the field scale, Phys. Rev. E. 71 (2005) 016311. https://doi.org/10.1103/PhysRevE.71.016311.
[27] V. Di Sarli, A. Di Benedetto, Modeling and simulation of soot combustion dynamics in a catalytic diesel particulate filter, Chem. Eng. Sci. 137 (2015) 69–78. https://doi.org/10.1016/j.ces.2015.06.011.
[28] ANSYS, ANSYS FLUENT 12.0 User's Guide - 7.2.3 Porous Media Conditions, (2012). http://www.afs.enea.it/project/neptunius/docs/fluent/html/ug/node233.htm (accessed March 8, 2018).
[29] COMSOL, Porous media, (2014). https://www.comsol.fr/.
[30] W.-C. Yang, Handbook of Fluidization and Fluid-Particle Systems, CRC Press, 2003.
[31] R. Boulesteix, A. Maître, J.-F. Baumard, C. Sallé, Y. Rabinovitch, Mechanism of the liquid-phase sintering for Nd:YAG ceramics, Opt Mater. 31 (2009) 711–715.
[32] R.M. German, Sintering Theory and Practice, 1st edition, Wiley-Interscience, New York, 1996.
[33] A. Goldstein, M. Katz, R. Boulesteix, Alexander.I. Shames, C. Coureau, J. Raetel, X. Mateos, L. Pavel, Sources of Parasitic Features in the Visible Range of Oxide Transparent

Ceramics Absorption Spectra, J Am Ceram Soc. 103 (2020) 4803–4821. https://doi.org/10.1111/jace.17182.
[34] M.N. Rahaman, Sintering of Ceramics, CRC Press Inc, 2007.
[35] W. Pabst, J. Hostaša, L. Esposito, Porosity and pore size dependence of the real in-line transmission of YAG and alumina ceramics, J. Eur. Ceram. Soc. 34 (2014) 2745–2756. https://doi.org/10.1016/j.jeurceramsoc.2013.12.053.